Q. J. R. Meteorol. Soc. (9999), **999**, pp. 101–118

Wave breaking and critical levels for propagating inertio-gravity waves in the lower stratosphere

By H. MOLDOVAN , F. LOTT and H. TEITELBAUM *
Laboratoire de Météorologie Dynamique, France

(Received 999; revised 999)

Summary

This paper analyses and interprets the formation of mixed layers due to propagating inertio-gravity waves observed during the FASTEX experiment. The data used are high vertical resolution soundings launched from different sites located in the North-Atlantic sector. In agreement with other studies, attributing the origin of the inertio-gravity waves to the adjustment of the jet-stream near fronts, the largest waves observed are often located in the vicinity and above frontal bands. The amplitude of these waves is large enough that they give rise to narrow mixed layers. By a detailed analysis of the waves characteristics, we can distinguish whether such a mixing is favored by the presence of an inertia-critical level, where $|\Omega| = f$ or results from a wave-induced convective instability occurring far from critical levels. Here, Ω is the wave intrinsic frequency and f is the Coriolis parameter. These observations highlight the importance of inertio-gravity waves in the vertical exchanges that occur in the stratosphere.

Keywords: Inertia-gravity waves Critical Levels Wave Breaking

1. Introduction

Inertio Gravity Waves (hereafter IGW) constitute a large part of the mesoscale motion spectrum of the atmosphere. They receive increasing attention because of the increasing observational capabilities and because they are assumed to play an important role in the transport of mass, momentum and trace constituents in the middle atmosphere. They have been observed over long periods of time with the MU radar by Fritts (1988) and Sato (1989) and many observational studies revealed that they can be generated in intense weather systems (Chan et al., 1991; Sato, 1993) in spite of the fact that the sources of IGWs can be difficult to identify because these waves can be large far from them (Ushimaru and Tanaka, 1990). The origin of gravity waves was further addressed by Nastrom and Fritts (1992) and Fritts

* Corresponding author: Laboratoire de Météorologie Dynamique, École Normale Supérieure, 24 rue Lhomond, 75231 Paris, France. E-mail: teitel@lmd.ens.fr.

and Nastrom (1992) who also found that these wave are large near mountains, fronts and convective cloud systems. The fact that IGWs are large near fronts is further supported Eckerman and Vincent (1993) who interpreted radar data as IGWs generated by cold fronts and by Moustaoui et al. (1999) who observed IGWs near fronts in the measurements of wind, ozone and water vapor done along the North Atlantic Flight Corridor during the POLINAT experiment.

There are many theories that explain the dynamical origin of IGWs. The mostly accepted is that IGWs result from an adjustment toward geostrophy of the large scale flow to an ageostrophic momentum forcing that comes either from fast disturbances generated by convection (Shutts and Gray, 1994) and mountains (Scavuzzo et al., 1998) or from slower synoptic disturbances as they start to develop fronts (Ley and Peltier, 1978; Gall et al. 1988; O'Sullivan and Dunkerton, 1995 ; Griffiths and Reeder 1996; Reeder and Griffiths 1996). Long IGWs can also result from direct orographic forcing or from non quasi geostrophic shear flow instabilities, that can occur when the minimum Richardson of the large scale flow is near and below 1 (Teitelbaum et al., 1987). In real cases, it is likely that these different mechanisms combine and it is difficult (or irrelevant) to identify the dominant one. For instance, a continuous spectra of IGWs can be generated by a mountain, and some modes can be amplified by the presence of a front (see Smith 1984 for the scale selection mechanism in the quasi-geostrophic case and Shen and Lin 1999 for the case with IGWs). Nevertheless, it is quite clear that for all the mechanisms listed above, the presence of a front favors the existence of large IGWs.

In addition to the generation of IGWs, it is also important to document their propagation and interaction with the large scale flow. It is indeed widely believed that they can transport momentum over great distances and deposit it at the levels where they are dissipated (Eliassen and Palm, 1961; Andrews and McIntyre, 1978). In the stratosphere, dissipation essentially occurs when the waves break (Lindzen, 1981) or/and when they encounter critical levels (Booker and Bretherton, 1967). At the levels where these processes occur, the waves also contribute to the mixing of the atmosphere through the small scale turbulence they can induce (Dunkerton, 1997; Teitelbaum et al, 1999). These different phenomena have been the subject of many theoretical and numerical studies but have not much been supported by observations. Until recently, as mentioned by Shutts and Gadian (1998), the vertical resolution in the dataset used to document IGWs was not high enough to detect these processes without ambiguity. Nowadays, the radio-soundings launched during some field experiments have very good vertical resolution and allow to observe atmospheric fluctuations of few tenth of meters in the vertical direction. They are thus capable to detect the narrow mixed layers that result from wave breaking or/and critical levels.

Since the detection of critical levels is an important aspect of our study it seems worthwhile to recall some of their properties. Early studies of gravity waves-critical level interaction have been made in the 2 dimensional case, without Coriolis force (Booker and Bretherton. 1967). In this context a steady linear undissipated wave has a singular point at z_0,

$$\Omega(z_0) = 0 \ , \tag{1}$$

where it is absorbed providing the Richardson number is large at z_0. It can be amplified when the minimum Richardson number in z_0 is below 0.25 (van Duin and Kelder, 1982 ; Teitelbaum and Kelder,1985; Eltayeb and McKenzie, 1975). The Coriolis parameter can modify very significantly these results (Jones, 1967; Yamanaka and Tanaka, 1984), introducing two other singular points,

$$\Omega(z_{\pm f}) = \pm f \tag{2}$$

which for IGWs generally surround z_0. In the following we will use the terminology of Shen and Lin (1999) and call z_0 a classical critical level (CCL) and $z_{\pm f}$ the two inertia critical levels (ICLs). In the presence of ICLs, long waves are generally absorbed at the first ICL they met, they can nevertheless be amplified as they interact with the shear layer when the minimum Richardson number is near and below 1 (Teitelbaum et al., 1987). In all cases, the wave amplitude and vertical wavenumber increase a lot when a disturbance approaches a critical level (CCL or ICLs).

In the 3 dimensional case (Shutts, 1995, 1998; Shutts and Gadian, 1998; Broad, 1999), the multiplicity of critical levels for a broad-band ensemble of waves, and when the wind veers with altitude can result in wave-mean flow interaction at near all altitudes. This can make critical levels difficult to identify, in the sense that they are present everywhere. In the cases selected in this paper, it does not seem to be the case, the waves present rather identifiable behavior in the horizontal direction so we can admit that they have a narrow spectrum.

The purpose of this paper is to provide a comprehensive interpretation of the vertical structure of IGWs generated in frontal zones. We will try to identify their source, describe their propagation and their breaking or their interaction with critical levels. All along the paper we will separate these last two phenomena. Conceptually, they are indeed rather different, since, on the one hand, wave breaking can occur in a background flow which does not vary with altitude. It results from that the waves can locally become large in amplitude and overturn as they propagate upward. On the other hand, the existence of critical levels necessarily implies that of a vertically varying background wind but does not necessarily imply intense convective overturning. For instance, for 2D monochromatic waves, it is the case when the critical level interaction is controlled by unsteadiness or dissipations rather than by nonlinearities (Lott and Teitelbaum, 1992). In reality however, for a wave to be detected without ambiguity, it needs to be quite large so there are good chances that it leads to convective overturning, near below the first critical level it meets.

This last point does not make the distinction between critical levels and wave breaking purely academical. Even if these two concepts sometime overlap in realistic situations, many robust differences can be listed. The most important one is that when a upward propagating wave breaks at a given altitude, and in the absence of critical levels, a significant fraction of its energy can still propagate upward. It is not the case when a wave encounter a critical level if the Richardson number of the flow near that level is larger than 1. Note that this result extents to strongly nonlinear critical level interaction, where intense wave breaking occurs that can locally decreases the large scale Richardson number below the critical level. It this case, some studies in the $f = 0$-case, have shown that the wave reflection can be increased up to near 1, while its transmission stays small (Clark and Peltier, 1984; Lott and Teitelbaum, 1992). Here and next in this paper we will restrict the terminology of "wave breaking" (WB) to the case where wave induced convective overturning occurs far from a critical level. It does exclude the cases where breaking occurs near a critical level. Situations where a critical level is detected are called "inertia critical level" (ICL), They can be identified even if breaking is not exactly observed in the sounding near below. Furthermore, we consider ICLs only because the waves we study are rather long and thus always encounter an ICL before they eventually reach a CCL. In other words, the waves are long enough that the distance between the ICLs and the CCL is significant.

The radiosoundings data we use have been collected during the Fronts and Atlantic Storm Track EXperiment (FASTEX ; Joly et al., 1997) during which cyclogenesis and fronts have been documented in great detail. These soundings have resolution up to 10m and the background flow conditions to which these soundings are related are issued from the European Center of Medium Weather Forecast (ECMWF) analysis. Section 2 derives the analytical diagnostic tools we use to describe IGW propagation, breaking (WB) and critical layer interaction (ICL) in real data. These diagnostics are derived in the non-dissipative case and for a mean flow that varies with height. Section 3 presents the experimental data used, and the series analysis techniques applied to them. Section 4 presents the results of the analysis of more than 60 soundings. Among them 3 representative cases are selected and discussed with great details. In these 3 cases, the soundings show mixed layers and well defined wave-form profiles. In this section the ECMWF analysis is used to identify the origin of the observed IGWs and to obtain information upon the waves horizontal structure. Results are summarized in Section 5.

2. Methodology and Mathematical background

It is well known that a decrease of the potential temperature gradient can be the signature of WB or CLs. Nevertheless, there are many other phenomena such as local shear instabilities, tropopause foldings or stratospheric laminae (Mariotti et al., 1997) that can induce such nearly mixed layers, and that are not related to waves. Thus to determine if a decreased potential temperature gradient can be attributed to IGWs dynamics we will check: (i) that the horizontal wind disturbances amplitude is significant compared to the total wind at the level (for WB) or just below the level (for ICL) of interest; (ii) that below this level, the horizontal wind disturbances extent over sufficient depth that we can attribute them to waves (by identifying a vertical wavenumber for instance) and (iii) that the hodograph of the disturbance horizontal wind turns with altitude, as it does for vertically propagating IGWs. Although they require careful data treatments, these 3 diagnostics only stand that IGWs and mixed layers can be observed simultaneously, they do not interpret by which processes (WB or ICLs) they are linked. To do so, for ICLs, we will check (iv) that the wave amplitude drops from the lower side of the ICL to the upper side; (v) that its vertical wavelength decreases as the wave approaches its ICL and (vi) that the wave horizontal wind components become nearly a quarter of cycle out of phase near an ICL. (vii) More simply, and using the wave dispersion relationship, together with information on the wave spatial structure deduced from the soundings and from the ECMWF analysis, we will compute the wave intrinsic frequency and check directly that we are in the presence of an ICL. (viii) To determine if the waves break away from a CL we will use a criteria linking the wave frequency, its horizontal wavenumber and the horizontal wind amplitude. As to our knowledge the diagnostics (vi) and (viii) are not much used, we derived them again in the next paragraphs.

(*a*) *Basic equations*

As most of the disturbances described in this paper behave like IGWs, we will use the hydrostatic and f-plane approximation. The hydrostatic assumption is valid if the vertical scale is much smaller than the horizontal one. It is justified for IGWs whose ratio between vertical and horizontal scales is small. We will also assume that the vertical profiles analyzed, can be considered as a superposition between a background flow and a disturbance. We will consider that the background horizontal velocity fields $U_0(z)$ and $V_0(z)$ vary with the log-pressure vertical direction $z = H \log(P_r/P)$ only (Holton, 1992). Here, H is a standard scale height, $H = RT_r/g$, T_r is a reference temperature, R is the Gas constant for dry air, g is the gravity and P_r is a reference surface pressure. In this context, the background geopotential, $\Phi_B(x, y, z)$ also varies with the horizontal directions x and y, according to the "horizontally integrated" thermal wind relationship,

$$\Phi_B(x, y, z) = \Phi_0(z) + xfV_0(z) - yfU_0(z) \ . \tag{3}$$

We will also assume that the disturbance field is of narrow band in both horizontal wavenumber and frequency domain, so that it is well described by a single harmonic disturbance with zonal wavenumber, k, meridional wavenumber, l, and absolute frequency, ω:

$$q'(x, y, z, t) = \Re \left(\hat{q}(z) e^{z/2H} e^{i(\omega t - kx - ly)} \right) \ . \tag{4}$$

In Eq. 4, the primes are used to identify the disturbance field. In this context, the equations for a disturbance write:

$$i\Omega\hat{u} - ik\hat{\phi} - f\hat{v} + \frac{dU_0}{dz}\hat{w} = 0 \tag{5a}$$

$$i\Omega\hat{v} - il\hat{\phi} + f\hat{u} + \frac{dV_0}{dz}\hat{w} = 0 \qquad (5b)$$

$$i\Omega(\frac{d\hat{\phi}}{dz} + \frac{\hat{\phi}}{2H}) + f\frac{dV_0}{dz}\hat{u} - f\frac{dU_0}{dz}\hat{v} + N_0^2\hat{w} = 0 \qquad (5c)$$

$$-ik\hat{u} - il\hat{v} - \frac{\hat{w}}{2H} + \frac{d\hat{w}}{dz} = 0 \qquad (5d)$$

where $\Omega = \omega - kU_0 - lV_0$ is the intrinsic (or Doppler-shifted) frequency and,

$$N_0^2 = \frac{\partial^2 \phi_0}{\partial z^2} + \frac{\kappa}{H}\frac{\partial \phi_0}{\partial z} \ , \qquad (6)$$

is the Brunt-Vaisala frequency. In Eq. 6 one has further neglected the dependence in x and y of N^2 coming from the integrated thermal wind relationship (3). As have shown Teitelbaum et al. (1987) this approximation is justified if the horizontal scale, L, of the disturbance is such that:

$$Lfg^{-1}|\frac{d\vec{U}_o}{dz}| << 1. \qquad (7)$$

A condition similar to that used implicitly by Jones (1967).

(*b*) *Polarization relationships and CL detection*

The fact that the disturbance horizontal wind components become more and more a quarter of cycle out of phase each other when an IGW approach an ICL (property (vi) in the list above), can be deduced from the polarization relationships, obtained from Eqs. (5a)-(5b) that link the horizontal velocity components to the geopotential and vertical velocity fields:

$$\hat{u} = \frac{1}{(\Omega^2 - f^2)}\left[\hat{\phi}(k\Omega - ifl) + \hat{w}\Big(i\Omega\frac{dU_0}{dz} + f\frac{dV_0}{dz}\Big)\right] \ , \qquad (8a)$$

$$\hat{v} = \frac{i}{(\Omega^2 - f^2)}\left[\hat{\phi}(kf - i\Omega l) + \hat{w}\Big(if\frac{dU_0}{dz} + \Omega\frac{dV_0}{dz}\Big)\right] \ . \qquad (8b)$$

The relations (8a) and (8b) show that $\hat{v} \to \pm i\hat{u}$ when $\Omega \to \pm f$, i.e. the phase difference between $\hat{u}$ and $\hat{v}$ approaches $\pm\pi/2$. This is a natural consequence of the decrease of the wave frequency with respect to the moving medium.

(*c*) *Linear wave breaking criteria*

The idea of convective WB involves the notion of a material surface becoming locally vertical before overturning, leading to breaking. When the flow is quasi-adiabatic, the isentropic surface are material and so we expect that at the breaking level the potential temperature becomes constant with altitude. Then, to find a criteria for WB, one has to derive an expression for the total potential temperature gradient. This can be done by writing the energy Eq. 5c using potential temperature and under the approximated form:

$$i\Omega\hat{\theta} + \frac{d\theta_0}{dz}\hat{w} = 0 \ . \tag{9}$$

In Eq. 9 the horizontal advection of the background temperature field, needed to satisfy the thermal wind balance (Eq. 3) has been neglected compared to Eq. 5c. This approximation is only valid for large background Richardson number. We verified that it is generally true in our soundings and in the stratosphere, i.e. essentially where we will use the criteria derived next. The Richardson number can nevertheless become rather small near the tropopause, i.e., near the level where we expect the waves to be generated. We then consider the vertical derivative of Eq. (9) and assume that the resulting equation is dominated by the terms involving perturbation vertical derivatives (Fritts, 1984). Taking also into account that, $\frac{d\hat{w}}{dz} >> \frac{\hat{w}}{2H}$ in Eq. (5d), the Eq. (9) can be transformed into:

$$\Omega\frac{d\hat{\theta}}{dz} + (k\hat{u} + l\hat{v})\frac{d\theta_0}{dz} = 0 \ . \tag{10}$$

Then, coming back to the physical space, to have the vertical derivative of the total potential temperature, $\theta_0 + \theta'$, equals to zero, we must have:

$$\Omega(z_b) = \Re\left((k\hat{u}(z_b) + l\hat{v}(z_b))e^{z_b/2H}e^{i(\omega t - kx - ly)}\right) \ .$$

This equation transforms into

$$\Omega(z_b) = ku'(x, y, z_b, t) + lv'(x, y, z_b, t) \quad \text{or} \quad \omega = ku(x, y, z_b, t) + lv(x, y, z_b, t) \tag{11}$$

In Eq. (11), $\vec{u} = \vec{U}_0 + \vec{u}'$ is the total wind and z_b is the WB altitude. In the following, we will consider that x, y and t are fixed and given by the sounding launching site and time respectively. Expression (11) is a useful diagnostic because it involves total horizontal winds which are directly measured quantities. The horizontal wavenumbers k and l nevertheless, need to be known. In the following, they will be obtained from the ECMWF analysis. In this evaluation of the breaking altitude, z_b, we have used hydrostatic linear theory to estimate wave breaking, which is an essentially non-hydrostatic nonlinear process. Although this can look contradictory, it is well known that such an approach often give quite good estimates (Bacmeister et al., 1994).

3. Data Processing

The methodology used to extract the waves and the background flow from the soundings consist in two main steps; first a cubic spline is applied to have equally spaced points with a resolution of 50 m. We choose 50 m for the resolution because the distance between the measured points varies around this value. Then a High-Pass filter is used to suppress all disturbances with vertical scale larger than 10 km. The filter is a non-recursive one, so the phase of the signal harmonics is conserved. It uses a Kaiser window (Hamming, 1983), whose parameters are adjusted to avoid Gibbs effects (for a more complete description of the filter and his transfer function, see Scavuzzo et al. (1998)). Except in some cases which will be indicated, we do not filter short disturbances in order to avoid the smoothing of very high horizontal wind gradient which can indicate the presence of an ICL. To consider only waves with vertical wavelength lower than 10 km is rather arbitrary, but, on the one hand, we are limited by the length of the sample and on the other hand, we are essentially interested in IGWs, whose vertical wavelength is in general significantly smaller than 10 km.

To quantify the variation with altitude of the wave vertical wavelength and that of the phase relation between the horizontal velocity components we will use a wavelet analysis. The wavelet transform of a space signal $f(z)$ is defined as

$$W_\psi(f)(a,b) = \frac{1}{\sqrt{a}} \int_{-\infty}^{\infty} f(z)\psi(\frac{z-b}{a})\, dz \tag{12}$$

where $\psi(z)$ is the basis wavelet, a is a dilation/compression-scale factor, and b represents the translation in space. For all the calculations we will use the Morlet wavelet (Morlet et al., 1982):

$$\psi(\frac{z-b}{a}) = \frac{1}{\sqrt{2a\pi}} e^{[-\frac{(z-b)^2}{2a^2}]} e^{[\frac{i\omega_o(z-b)}{a}]} \tag{13}$$

where the parameter ω_o determines the number of oscillations of the wavelet. Then for a given b (altitude) the local wavelength is deduced from the value of a for which the wavelet transform has the maximum amplitude (Torresani, 1995). The relative phase between the horizontal wind components corresponds to the phase difference between their wavelet transform.

4. Experimental results

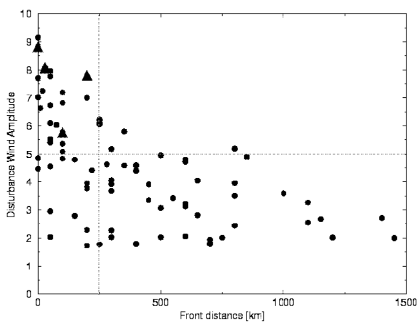

Figure 1. Disturbance wind amplitude evaluated with 60 vertical soundings launched during FASTEX as a function of the closest front distance. Triangles indicate the soundings analyzed in the 3 cases study.

The soundings analyzed with details in this section are selected among an ensemble of more than 60 soundings launched at Angssalik (65.5N, 37.6W), Narssarssuaq (61.2N, 45.4W) and Egedessmind (68.4N, 52.2W). For each sounding the wave signal is systematically extracted from the horizontal wind components, using the 10 km High-Pass filter described before and the potential temperature profile is analyzed to detect mixed layers. In all cases, we examine the associated synoptic tropopause conditions and determine if the sounding is located close or far from an upper level front. To do this, we evaluate the horizontal distance between the sounding and the place where the 150 hPa temperature horizontal gradient is maximum.

Figure 1 shows the amplitude A of the disturbance signal extracted, as a function of the distance D to the nearest front, and for the soundings ensemble mentioned above. In Fig. 1, the wave amplitude A is evaluated as

$$(Z_{max} - Z_{min})A^2 = \int_{Z_{min}}^{Z_{max}} (u'^2 + v'^2)\, dz \qquad (14)$$

where $Z_{min} \approx 13\, km$ to insure that the waves analyzed are well located in the low stratosphere and Z_{max} is the maximum altitude the sounding reaches. u' and v' are the 10 km High-Pass horizontal wind components. Figure 1 clearly illustrates that disturbances are large when they are near a front. For all these soundings we selected those for which the wave amplitude is quite large, and analyzed the associated mixed layers. The strategy used to do so is presented with great details in the three following cases, which we consider as very representative of what we observed in nearly all the

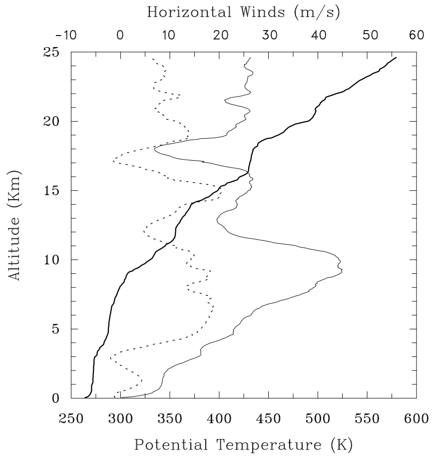

Figure 2. Vertical Profiles of the zonal wind (thin solid line), meridional wind (dotted line) and potential temperature (thick solid line) observed in a vertical sounding. Angssalik (65.6N, 37.6W), 19 January 1997 at 2300 UTC.

soundings where the wave signal is large. Nevertheless, among the soundings we could have selected, those we chose belong to a sub-ensemble of events where the nearest front presents large scale oscillations. These oscillations have horizontal scales large enough that they are properly resolved by the T213 ECMWF analysis, giving some confidence in their realism. In the following we will assume that these large scale horizontal disturbances organize, and result from, the frontal ageostrophic dynamics, so that they are related somehow to the waves observed aloft in the soundings.

(*a*) *Case 1*

Figure 2 shows the potential temperature and horizontal wind profiles deduced from the Angssalik (65.6N, 37.6W) sounding launched the 19 January 1997 at 23 UTC. The horizontal velocity profiles show strong oscillations between 10 km and 20 km and the potential temperature profile presents three marked layers of reduced gradients in this zone (11-12 km, 16-18 km and 20-21 km) and at least two others where it is slightly reduced (for instance 19 km). The upper tropospheric conditions this day are displayed on Fig. 3, which shows the temperature and the ageostrophic wind at 150 hPa (≈ 12 km) pressure surface issued from the ECMWF analysis of the 20 January 1997 at 00 UTC. This map shows an upper level front located close the launching site with an intense ageostrophic wind component. Figure 3 also shows that the temperature field and the ageostrophic wind present few oscillations along the front. Although the ECMWF anal-

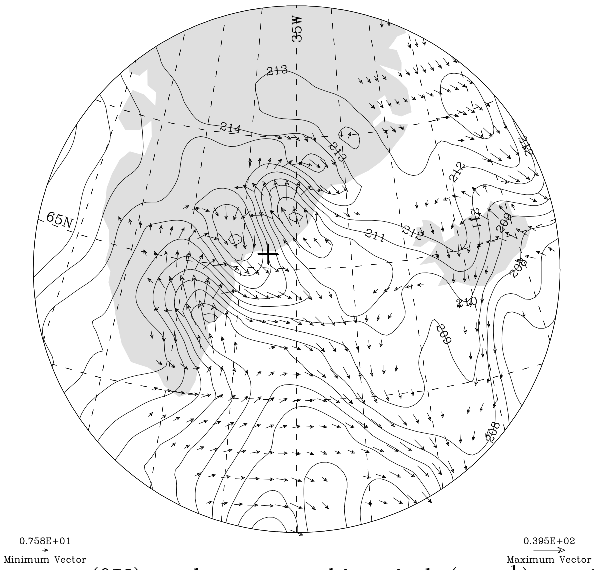

Figure 3. Temperature (°K) and ageostrophic wind (ms^{-1}) at 150 hPa from the ECMWF analysis. Contour interval for temperature=1°K. Arrows length proportional to wind speed (Maximum and Minimum values indicated at the figure bottom). The thick cross locates Angssalik. 20 January 1997 at 0000 UTC.

ysis have a reputation for quality at the synoptic scales (see for instance Moustaoui et al., 1999) it can not be excluded that these oscillations are overstated here compared to reality. They can result from the adjustment of the model to the introduction of sparse data or as a model response to the Greenland forcing. Figure 3 nevertheless indicates that the synoptic flow this day has a natural dynamical tendency to give rise to long, along front waves. The mechanism by which this wavenumber is selected can be closed to that giving rise to long IGW resonant overreflection, in a vertically stratified rotating shear flow, when the minimum Richardson number is near and below 1 (Teitelbaum et al., 1987). This mechanism can also explain the presence of a narrow spectrum. These waves, by forcing undulations in the frontal surface, provide the horizontal scale for the waves above the front.

To isolate better this oscillatory structures from the large scale quasi-geostrophic flow, we have computed the horizontal velocity divergence at 150 hPa from the ECMWF analysis (not shown here, but see case 2, where this field is presented instead of the upper level temperature field). It shows a wave structure very similar to that found on the temperature field. It has an horizontal wavelength of 550 km approximately that makes an angle of 55° approximately with the zonal direction.

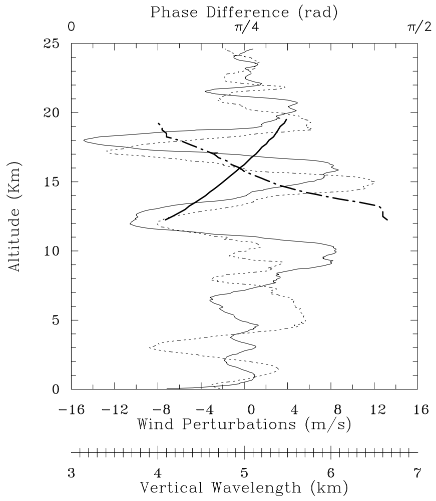

Figure 4. Vertical profiles of the disturbance zonal wind (thin solid line), meridional wind (thin dotted line), local vertical wavelength (thick dotted dashed) and wind components phase difference (thick solid). Angssalik (65.6N, 37.6W), 19 January 1997 at 2300 UTC.

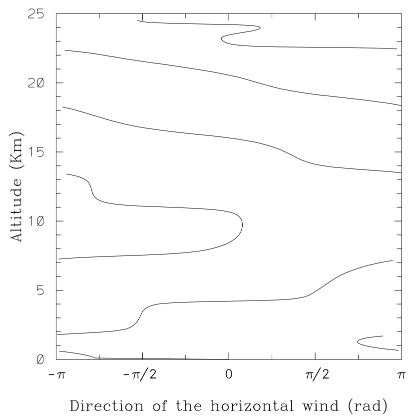

Figure 5. Vertical profile of the angle of the wind. Angssalik (65.6N, 37.6W), 19 January 1997 at 2300 UTC.

Figure 4 shows the vertical profiles of the High-Pass filtered wind components. It shows that the disturbance amplitude is large everywhere and presents well defined oscillations which amplitude exceed 10m s^{-1} on both u' and v' in the low stratosphere (between 13 km and 19 km). Here the wind components have comparable amplitude and seems to be in phase lag indicating that the signal is dominated by a vertically propagating IGW. To check this point further and to try to detect vertically propagating waves, we next filter the wind data in the 3-9 km window and compute the wind vector angle. The result is displayed in Fig. 5 which shows a clockwise rotation above 11 km and anti-clockwise below. This last result comforts the hypothesis that IGWs are generated at the front and propagate upward and downward from there.

The behavior of the disturbance wind fields near 19 km altitude is of great interest (Fig. 4). Indeed, both u' and v' components present very strong gradients there, and they are close from being a quarter of cycle out of phase each other. Furthermore, the disturbance amplitude drops sharply above this altitude, and we recall that the potential temperature is slightly reduced there (Fig. 2). All these results are consistent with that we are in the presence of an IGW interacting with an ICL. To quantify this more precisely, we next make the wavelet transform of the disturbance wind components. It is also displayed in Fig. 4 which shows the variation of the vertical wavelength with altitude and the phase difference variation between u' and v'. This result confirms what we have intuited from the direct observation of the wind profiles, i.e. that the wavelength of the disturbance decreases when approaching 19 km and that u' and v' become more and more a quarter of cycle out of phase.

Nevertheless, some limitations of the wavelet spectrum analysis should be pointed out. On the one hand, the lack of data outside our space span introduces an edge effect which is less important for small values of ω_0. On the other hand, the determination of the local wavelength is more accurate for rather large values of ω_o (Eq. (12)). Accordingly, we made sensitivity tests and found that ω_o near the standard value ($\pi\sqrt{2/ln2}$) give the best results considering the commitment between both limitations. These tests also suggest that we make an error of about 15% in the determination of the vertical wavelength.

Until now, we have not tried to link the mixed layers at 11-12 km, 16-18 km and 20-21 km to the waves observed in the soundings. A reason is that among these three layers only that around 17.5 km can reasonably be related to the waves. At this altitude we are indeed located far above the tropopause and the waves are large. The occurrence of a mixed layer at 11-12 km is certainly related to the presence of the upper level front, where the ageostrophic dynamics can decrease the potential temperature vertical gradient and give rise, through small scale turbulence, to mixed layers similar to that observed in Fig. 2. The mixed layer at 20-21 km can not be related to the waves observed at that time because the waves are very small around 20-21 km: they are attenuated at the critical level located below (around 19 km). As we will show in the case 2, it is probably related to the IGW breaking observed 6 hours before upwind at this altitude.

To confirme that the WB and the CL are well located at $z_b = 17.5$ km and $z_{\pm f} = 19$ km, respectively we use next the conditions found in Section 2. From the ICL definition (Eq. (2)) and the WB criteria (Eq. (11)) the following relation can be obtained,

$$\frac{\vec{k}}{|\vec{k}|} \cdot (\vec{u}(z_b) - \vec{U_0}(z_{\pm f}) = \pm \frac{f}{|\vec{k}|} \ . \tag{15}$$

From the soundings and using for the mean flow the Low-Pass wind that remains from the filtering processes we found, $\vec{u}(z_b) = (13.2, 1.5)$ ms^{-1} and $\vec{U_0}(z_{\pm f}) \approx (21, 11)$ ms^{-1}. Using the value of $\vec{k}$ deduced from ECMWF analysis the right hand side and the left hand side of Eq. (15) give

$$\frac{\vec{k}}{|\vec{k}|} \cdot (\vec{u}(z_b) - \vec{U_0}(z_{\pm f})) \approx -12.3 \ ms^{-1} \quad \text{and} \quad \pm \frac{f}{|\vec{k}|} \approx \pm 11.5 \ ms^{-1} \tag{16}$$

($f \approx 1.32 \ 10^{-4}$ at 65N), respectively, and providing we choose the horizontal wavenumber zonal component positive. These two values agree reasonably well if the ICL altitude is that for which the wave intrinsic frequency equals $-f$, i.e., the ICL is located at $z_{-f} = 19 \ km$.

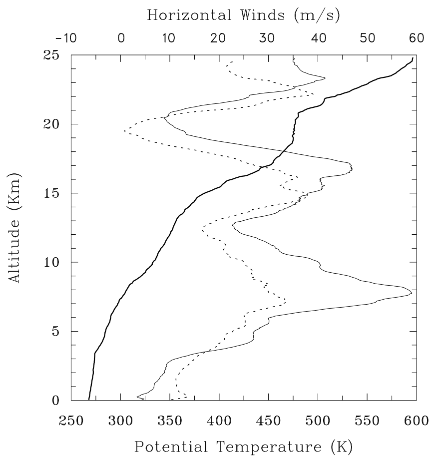

Figure 6. Same as Figure 2. Narssarssuaq (61.2N,45.4W), 19 January at 1730 UTC.

The fact that we found an ICL provides further information upon the horizontal direction of wave propagation. For the horizontal wavenumber pointing toward the North-West, the mean wind projected along that direction decreases with height between the tropopause and 18-20 km. That the disturbance propagates vertically in such a background and encounter an ICL means that its intrinsic frequency Ω increases from negative values up to $-f$ when z varies from the generation level up to the lowest ICL : the wave propagates toward the South-West against the mean wind.

A quite independent cross checking of the altitude of the WB consist in evaluating Ω at a given altitude located away from a critical level by using the dispersion relation,

$$\Omega^2 = f^2 + \frac{N^2 k^2}{m^2} \ , \tag{17}$$

the local vertical wavelength being provided by the wavelet analysis. At $z_b = 17.5$ km the wavelet analysis gives $\lambda_z = 2\pi/m \approx 4.2$ km. For this value and using Eq. (17) we found $\Omega(z_b) \approx 1.8\ 10^{-4} s^{-1}$. This value can be compared to that using Eq. (11): $\Omega(z_b) \approx 1.6\ 10^{-4} s^{-1}$. This good matching reinforces that the very low potential temperature gradient corresponds to WB. This double check, plus the fact that the first matching Eq. (15) needs the altitude of the CL, is an a posteriori confirmation that we located the CL at the correct place.

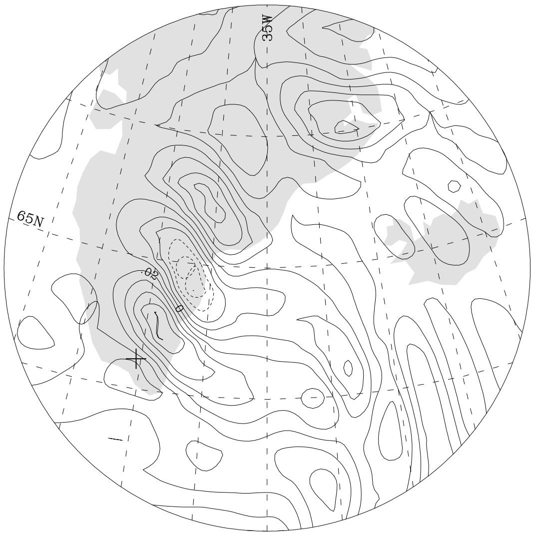

Figure 7. Horizontal velocity divergence at 150 hPa from the ECMWF analysis. CI=$210^{-5}s^{-1}$, negative values are dashed. The thick cross locates Narssarssuaq. 19 January at 1800 UTC.

(b) Case 2

Figure 6 shows the potential temperature and horizontal wind components deduced from the Narssarssuaq (61.2N, 45.4W) sounding launched the 19 January 1997 at 1730 UTC (i.e., 6 hours before the sounding analyzed in Case 1). As in case 1, the velocity profiles show large oscillations. In the stratosphere they dominate the wind field from 12 km altitude to the sounding top. The potential temperature profile shows a thick layer of

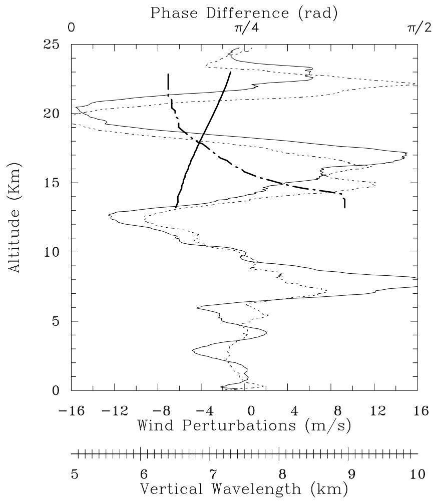

Figure 8. Same as Figure 4. Narssarssuaq (61.2N,45.4W), 19 January at 1730 UTC.

very low, almost zero, potential temperature gradient around 20 km. In this sounding we can also note that the maximum amplitude of the wind perturbation appears at the same altitude as the low potential temperature gradient suggesting that we are in the presence of WB. As in the previous case, we want to give further dynamical evidences that it is the case.

Figure 7 displays the horizontal wind divergence at 150 hPa level obtained from ECMWF analysis at 18 UTC on the same day. The trace of a frontal oscillation is clear, it allows to deduce an horizontal wavelength of 550 km approximately that makes an angle of 60° with the zonal direction. Regarding the degree of approximation in these wave vectors evaluation we can consider that the frontal wave structure is the same as in case 1: we can thus consider that we are in the presence of the same wave. Regarding the vertical soundings, this is not as clear because the wind perturbations profile (Figures 4 and 8) are very different above 19 km (they are very similar below). As seen before, this difference can be explained by the fact that the large scale wind profiles which control the wave structure are different somehow: at Angssalik 6 hours later (case 1) this wave encounters a CL at 19 km.

The vertical wavelength is deduced from the wavelet analysis and is displayed in Fig. 8 as well, together with the phase difference between the horizontal wind components. At the altitude where we suspect that the wave breaks, i.e. near $z_b = 20$ km, $\lambda_z \approx 6.3$km. Using the dispersion relation (17) we obtain $\Omega(z_b) = -2.3\ 10^{-4}s^{-1}$ and the frequency deduced assuming that the breaking criteria (11) is satisfied gives $\Omega = -2.2\ 10^{-4}s^{-1}$. This confirm that we can attribute the low potential temperature gradient found at 20 km to the breaking of the wave, if we admit again that the wave propagates to the South-West. Note there that it is the mixed layer we refer to in case 1, to explain the 20 km layer of reduced vertical gradient of potential temperature observed at Angssalik 6 hours later.

The existence of a CL in this case is difficult to assess, because it is probably located at the upper end of the sounding where the data are less reliable. In any case, we can say that around 22 km altitude there is a thin layer where the potential temperature has a low gradient and above it the wind perturbation seems to strongly decrease.

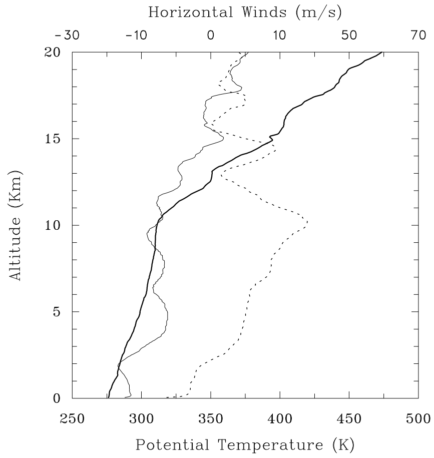

Figure 9. Same as Figure 2. Angssalik (65.6N, 37.6W), 1 January 1997 at 2300 UTC.

(*c*) *Case 3*

Figure 9 shows the potential temperature and horizontal wind profiles measured by the Angssalik (65.6N, 37.6W) sounding launched the 1rst January 1997 at 23 UTC. The horizontal velocity profiles show wave like perturbations and the potential temperature profile displays three nearly

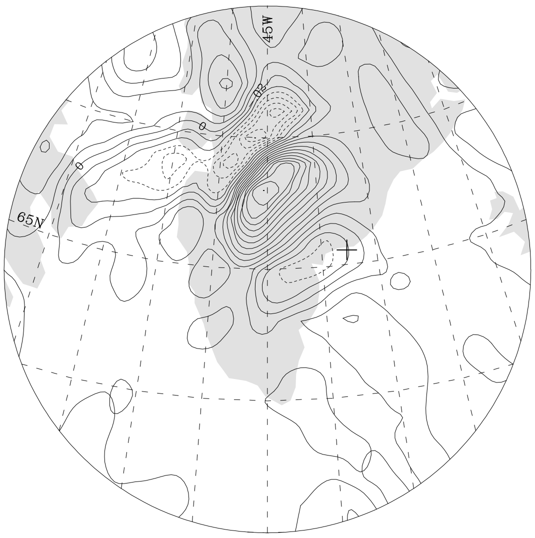

Figure 10. Same as Figure 4. The Thick Cross locates Angssalik. 2 January 1997 at 0000 UTC.

mixed layers at 13, 16, and 18 km respectively. The upper level Tempera-

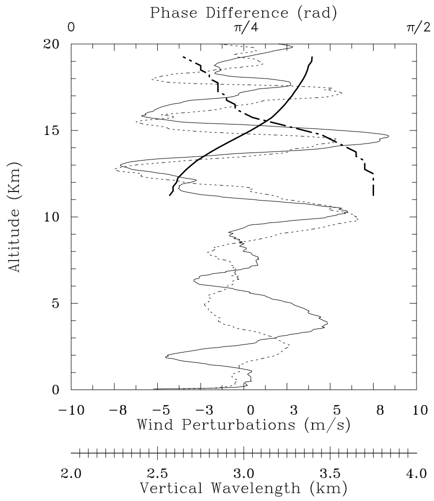

Figure 11. Same as Figure 5. Angssalik (65.6N, 37.6W), 1 January 1997 at 2300 UTC.

ture field this day, presents an ondulating front, oriented from North-West to South-East, and that crosses the Greenland Plateau (not shown). As indicate the 200 hPa horizontal velocity divergence field (Fig. 10) this front presents a well defined oscillation with approximate horizontal wavelength $\lambda_H \approx 550$km, and angle $\alpha \approx 120°$ with respect to the zonal direction. Figure

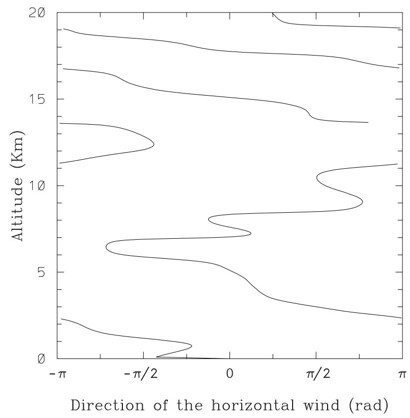

Figure 12. Same as Figure 6. Angssalik (65.6N, 37.6W), 1 January 1997 at 2300 UTC.

11 shows the two components of the horizontal wind perturbations after a rotation of 45°. Figure 11 also displays the vertical variation of their phase difference, and the local vertical wavelength of the zonal wind calculated using the wavelet transform. The facts that (i) the horizontal wind disturbance amplitude is large that (ii) it drops significantly above 18 km, that (iii) the vertical wavelength decreases as approaching this level and that (iv) the phase difference between u' and v' approaches 90° strongly suggest that we are in the presence of a CL. Furthermore, the fact that the disturbance is presumably generated at the upper front altitude is confirmed by the Fig. 12 which shows the rotation of the wind vector perturbation with altitude. Above that level the hodograph turns clockwise indicating waves propagating upward from the level $z = 12$ km (i.e., approximately 200 hPa).

To check more dynamically that there is a ICL at $z_{\pm f}$ =18 km, we will use the ICL definition (2). Therefore, we need to know the intrinsic frequency at this level. To do so, from the dispersion relation (17) evaluated with the vertical wavelength at $z_{15} = 15$ km and the horizontal wavenumber evaluated from the ECMWF analysis, we obtain $\Omega(z_{15})$. Then, using the expression

$$\Omega(z_{\pm f}) = \Omega(z_{15}) + \vec{k}(\vec{U}(z_{15}) - \vec{U}(z_{\pm f})) \tag{18}$$

we deduce that $\Omega(z_{\pm f}) \approx 1.2\ 10^{-4}s^{-1}$ providing the IGW propagates toward the South-East. This value compared well with the value of f at this latitude ($f \approx 1.32s^{-1}$) confirming the existence of an ICL. Furthermore, Ω decreases with height up to the ICL, in accordance with the mean wind variation.

Figure 9 shows another two layers, around 13 km and 16 km, where the vertical gradient of potential temperature is very weak. The highest layer is probably a consequence of the temperature variation induced by the wave. Nevertheless, the application of the WB criteria shows that the amplitude of the wave at 16 km is not large enough to induce convective instability. Finally, the 13 km layer is located in the frontal zone where, the decrease of the potential temperature gradient is certainly related to local frontal dynamics.

5. Discussion

To provide observational evidences that Inertia-Gravity Waves play an active role in the vertical irreversible mixings that occur in the low polar stratosphere, we have analyzed high resolution soundings launched during the FASTEX campaign. In these soundings we extracted a disturbance signal by high-pass filtering the wind data. In many circumstances, the rotation of the horizontal wind components with altitude indicates the presence of vertically propagating IGWs. Providing there is an Upper level front close the launching site, this kind of waves can dominate the unfiltered horizontal wind profiles at altitudes ranging from 13 km to 20 km typically (i.e., above the tropopause and up to the highest level of observation). In the same soundings we have analyzed the potential temperature profiles and observed mixed and/or nearly mixed layers quite systematically. When IGW can be characterized without ambiguity, these layers are located (i) near the tropopause, (ii) where the waves are large and (iii) just above a level where the disturbance amplitude drops sharply. In circumstance (iii) we also observed that the disturbance vertical wavenumber increases when approaching the layer of reduced potential temperature gradient and the horizontal wind components approach phase quadrature one with the other. To our knowledge, this last behavior of IGWs near ICLs has never been described in real case studies. From these findings it seems reasonable to attribute the mixed layers in (i) to local upper front ageostrophic dynamics, in (ii) to IGWs breaking and in (iii) to IGWs-ICL interaction. All the four cases presented in the paper illustrate at least two of these processes. These 3 cases (but others could have been chosen) also have in common that the close upper level front presents coherent and long along front oscillations. Since the waves we observed aloft are in essence quite long (hodographs for instance indicate that they are IGWs) it seems natural to associate the along front horizontal oscillations to the waves observed in the vertical soundings. When doing so, and using various diagnostics derived from the linear theory of IGWs propagating in a vertically varying background, we provide further dynamical evidences that the near mixed layer we do frequently observed in the low stratosphere are due to the presence of ICLs or to WB far from critical levels.

Acknowledgement

We acknowledge the scientific staff of CNRM and the Joint Office for Science Support for the free access to FASTEX data. We are thankful to ECMWF for the free access to their archives.

References

Andrews, D. G. and McIntyre, M. E. 1978 An exact theory of nonlinear waves on a Lagrangian-mean flow. *J. Fluid Mech.*, **89,** 609–646

Bacmeister, J. T., Newman, P. A., Gary, B. L. and K. R. Chan 1994 An algorithm for forecasting wave-related turbulence in the stratosphere. *Weather and Forecasting*, **9,** 2–20

Booker, J. R. and Bretherton, F. P. 1967 The critical layer for internal gravity waves in shear flow. *J. Fluid Mech.*, **27,** 513–539

Broad, A. S. 1999 Do orographic gravity waves break in flows with uniform wind direction turning with height? *Q. J. R. Meteorol. Soc.*, **125,** 1695–1714

Chan, K., et al. 1991 Horizontal wind fluctuation in the stratosphere during large-scale cyclogenesis. *J. Geophys. Res.*, **96,** 17425–17432

Clark, T. L., and W. R. Peltier 1984 Critical level reflection and the resonant growth of nonlinear mountain waves. *J. Atmos. Sci.*, **41,** 3122–3134

Dunkerton, T. J. 1997 Shear Instability of Internal Inertia-Gravity Waves. *J. Atmos. Sci.*, **54,** 1628–1641

Eckerman, S. D. and Vincent, R. A. 1993 VHF radar observations of gravity wave productions by cold fronts over southern Australia. *J. Atmos., Sci.*, **50,** 785–806

Eliassen, A. and Palm, E. 1961 On the transfer of energy in stationary mountain waves. *Geophys., Pub.*, **22,** 1-23

Eltayeb, I. A. and McKenzie, J. F. 1975 Critical level behavior and wave amplification of a gravity wave incident upon a shear layer. *J. Fluid Mech.*, **72,** 661–671

Fritts, D. C. 1988 Gravity wave saturation in the middle atmosphere: A review of theory and observations. *Reviews of Geophysics and Space Physics*, **22,** 275–308

Fritts, D. C. and Nastrom, G. D. 1992 Sources of mesoscale variability of gravity waves. Part II: Frontal, convective, and jet stream excitation. *J. Atmos. Sci.*, **49,** 111–127

Gall, R., et al. 1988 Gravity waves generated during Frontogenesis. *J. Atmos. Sci.*, **45,** 2204–2219

Griffiths, M. and Reeder, M. J. 1996 Stratospheric inertia-gravity waves generated in a numerical model of Frontogenesis. I: Models solutions. *Q. J. R. Meteorol. Soc.*, **122,** 1153–1174

Hamming R. W. 1983 *Digital Filters*, Englewood Cliffs: Prentice-Hall

Holton J. R. 1992 *An introduction to Dynamics Meteorology* 3^{rd} **Edition** Academic Press, New York

Joly, A. and 19 co-authors 1997 The fronts and Atlantic storm-track experiment (FASTEX): Scientific objectives and experimental design. *Bull. Am.Meteorol. Soc.*, **78,** 1917–1940

Jones, W. L. 1967 Propagation of internal gravity waves in fluids with shear flow and rotation. *J. Fluid Mech.*, **30,** 439–448

Keyser, D. and Shapiro, M. A. 1986 A review of the structure and dynamics of upper-level frontal zones. *Mon. Wea. Rev.*, **114,** 452–499

Ley, B. and Peltier, W. R. 1978 Wave generation and frontal collapse. *J. Atmos. Sci.*, **35,** 3–17

Lott, F. and Teitelbaum, H. 1992 Nonlinear dissipative critical level interaction in a stratified shear flow: instabilities and gravity waves. *Geophys. and Astrophys. Fluid Dynamics* **66,** 133–167

Lindzen, R. S. 1981 Turbulence and stress owing to gravity wave and tidal breakdown. *J. Geophys. Res.*, bf 86, 9707–9714

Mariotti, A., Moustaoui, M., Legras, B. and Teitelbaum, H. 1997 Comparition between vertical ozone soundings and reconstructed potential vorticity maps by contour advection with surgery. *J. Geophys. Res.*, **102,** 6131–6142

Morlet, J., Arehs, G., Fourgeau, I. and Giard, D. 1982 Wave propagation and sampling theory. *Geophysics*, **47,** 203–236

Moustaoui, M., Teitelbaum, H., van Velthoven, P. F. J. and Kelder, H. 1999 Analysis of gravity waves during the POLINAT experiment and some consequences for stratospheric-tropospheric exchange. *J. Atmos. Sci.*, **56,** 1019-1030

Nastrom, G. D. and Fritts, D. C. 1992 Sources of mesoscale variability of gravity waves. Part I: Tropospheric excitation. *J. Atmos. Sci.*, **49,** 101-110

O'Sullivan, D. and Dunkerton, T. J. 1995 Generation of inertia- Gravity Waves in a Simulated Life Cycle of Baroclinic Instability. *J. Atmos. Sci.*, **52,** 3695-3716

Reeder, M. J. and Griffiths, M. 1996 Stratospheric inertia-gravity waves generated in a numerical model of frontogenesis. II: Wave sources, generation mechanisms and momentum fluxes. *Q. J. R. Meteorol. Soc.*, **122,** 1175–1195

Sato, K. 1989 An inertial gravity wave associated with a synoptic- scale pressure trough observed by the MU radar. *J. Meteror. Soc. Japan*, **67,** 325–324

Sato, K. 1993 Small-scale wind disturbances observed MU radar during the passage of Typhoon Kelly. *J. Atmos. Sci.*, **50,** 518–537

Scavuzzo, C. M., Lamfri, M. A., Teitelbaum, H. and Lott, F. 1998 A study of the low-frequency inertio-gravity waves observed during the Pyrénés experiment. *J. Geophys. Res.*, **103,** 1747–1758

Shen, B. W. and Lin, Y. L. 1999 Effects of critical levels on two dimensional backsheared flow over isolated mountain ridge on an f-plane. *J. Atmos. Sci.*, **56,** 3286–3302

Shutts, G. J. and Gray, M. E. B. 1994 A numerical modelling study of the geostrophic adjustment process following deep convection. *Q. J. R. Meteorol. Soc.*, **120,** 1045–1078

Shutts, G. J. 1995 Gravity-wave drag parametrization over complex terrain: The effect of critical level absorption in directional wind shear. *Q. J. R. Meteorol. Soc.*, **121,** 1005–1021

Shutts, G. J. 1998 Stationary gravity wave structure in flows with directional wind shear. *Q. J. R. Meteorol. Soc.*, **124,** 1421–1442

Shutts, G., J. and Gadian, A. 1998 Numerical simulations of orographic gravity waves in flows which back with height. *Q. J. R. Meteorol. Soc.*, **124,** 1-37

Teitelbaum H., Moustaoui M., Sadourny R. and Lott F. 1999 Critical levels and mixing layers induced by convectively generated gravity waves during CEPEX. it/ Q. J. R. Meteorol. Soc., **125,** 1715–1734

Teitelbaum H. and Kelder, H. 1985 Critical levels in a jet-type flow. *J. Fluid Mech.*, **159,** 227–240

Teitelbaum H., Kelder, H. and van Duin, C. A. 1987 Propagation of internal gravity waves in a rotating fluid with shear flow. *J. Atmos. Terres. Phys.*, **49,** 413–420

Torresani, B. 1995 Analyse continue par ondelettes. *EDP Sciences*, **CNRS Editions,** 256p

Ushimara, S. and Tanaka, H. 1990 Characteristics of internal inertial gravity waves and inertial waves in the lower stratosphere observed by the MU radar. *J. Meteor. Soc. Japan*, **68,** 1–18 van Duin, C. A. and Kelder, H. 1982 Reflection properties of internal gravity waves incident upon a hyperbolic tangent shear layer. *J. Fluid Mech.*, **120,** 505–521

Yamanaka, M. D. and Tanaka, H. 1984 Propagation and breakdown of inertio gravity waves near critical levels in the middle atmosphere. it J. Meteor. Soc. Japan, **62,** 1–16